3D involute gear evaluation - part II: deviations - basic algorithms for modern software validation

OPEN ACCESS
IOP Publishing
Measurement Science and Technology
Meas. Sci. Technol. **33** (2022) 125003 (14pp)
https://doi.org/10.1088/1361-6501/ac8c60

3D involute gear evaluation - part II: deviations - basic algorithms for modern software validation

Martin Stein* **and Frank Härtig**

Physikalisch-Technische Bundesanstalt, Bundesallee 100, 38116 Braunschweig, Germany

E-mail: martin.stein@ptb.de

Received 17 March 2022, revised 8 August 2022
Accepted for publication 24 August 2022
Published 7 September 2022

Abstract

The fundamental equations for the evaluation of cylindrical involute gear measurements on 3D gear measuring instruments are provided. The computations are based on the principles of gear kinematics and use the system of involute gear coordinates introduced in a previous work of the authors. This holistic approach focuses on significant error sources that only appear since 3D measurement technology is used and that are almost unrecognized till today. The proposed algorithms are beneficial for the description of gear deviations as they allow the use of simple formulas covering profile, helix and pitch evaluation for internal or external and spur or helical gears. The presented equations contain the key fundamentals to complement existing standards. They will become part of reference algorithms used by the Physikalisch-Technische Bundesanstalt, the national metrology institute of Germany, to certify gear evaluation software.

Keywords: certification for involute gear evaluation, gear evaluations, software test, involute gear evaluation, 3D involute gear deviations

(Some figures may appear in colour only in the online journal)

* Author to whom any correspondence should be addressed.

Nomenclature

Symbol	Name	Range	Unit
b	Facewidth	$\in \mathbb{R}^+$	mm
c	Helix coefficient	$\in \mathbb{R}_0^+$	—
d_b	Base diameter	$\in \mathbb{R}^+$	mm
`flank`	Tooth flank direction	$\begin{cases} -1 & \text{: left} \\ +1 & \text{: right} \end{cases}$	—
F_α	Total profile deviation	$\in \mathbb{R}_0^+$	mm
F_β	Total helix deviation	$\in \mathbb{R}_0^+$	mm
$f_{f\alpha}$	Profile form deviation	$\in \mathbb{R}_0^+$	mm
$f_{f\beta}$	Helix form deviation	$\in \mathbb{R}_0^+$	mm
$f_{H\alpha}$	Profile slope deviation	$\in \mathbb{R}$	mm
$f_{H\beta}$	Helix slope deviation	$\in \mathbb{R}$	mm
F_p	Cumulative pitch deviation	$\in \mathbb{R}_0^+$	mm
f_p	Single pitch deviation	$\in \mathbb{R}_0^+$	mm
$F_{p,i}$	Individual cumulative pitch deviation	$\in \mathbb{R}$	mm
$F_{p,i}^v$	Individual cumulative pitch deviation at v-circle	$\in \mathbb{R}$	mm
$f_{p,i}$	Individual single pitch deviation	$\in \mathbb{R}$	mm
$F_{r,i}$	Individual runout value	$\in \mathbb{R}_0^+$	mm
F_r	Runout deviation	$\in \mathbb{R}_0^+$	mm
f_y	Deviation	$\in \mathbb{R}$	mm
f_y^{res}	Residual	$\in \mathbb{R}$	mm
`hand`	Slope direction of tooth	$\begin{cases} -1 & \text{: left} \\ 0 & \text{: spur} \\ +1 & \text{: right} \end{cases}$	—
i	Tooth number	$\in \mathbb{N}^+$	—
inv α	Involute α	$\in \mathbb{R}_0^+$	rad
L_α	Regression range for profile evaluation	$\subset \mathbb{R}_0^+$	mm
L_{AE}	Reference length for $f_{H\alpha}$	$\in \mathbb{R}_0^+$	mm
L_β	Regression range for helix evaluation	$\subset \mathbb{R}_0^+$	mm
l_y	Length of roll	$\in \mathbb{R}_0^+$	mm
m	Slope of regression line	$\in \mathbb{R}$	mm
M_{dK}	Dimension over (or between) balls	$\in \mathbb{R}_0^+$	mm
m_n	Normal module	$\in \mathbb{R}^+$	mm
M_{rK}	Radial single-ball dimension	$\in \mathbb{R}_0^+$	mm
n	Number of teeth	$\in \mathbb{N}^+$	—
n_z	z-component of normal vector on involute surface	$\in \mathbb{R}$	—
p_i	Measurement point	$\in \mathbb{R}^3$	mm
r	Radius	$\in \mathbb{R}^+$	mm
r_b	Base radius	$\in \mathbb{R}^+$	mm
r_s	Radius of stylus tip	$\in \mathbb{R}^+$	mm
r_v	Radius of v-circle	$\in \mathbb{R}^+$	mm
r_0	Radius of reference circle	$\in \mathbb{R}^+$	mm
s_{t0}	Tooth thickness at reference circle in transverse section	$\in \mathbb{R}^+$	mm
`type`	Type of gear	$\begin{cases} -1 & \text{: internal} \\ +1 & \text{: external} \end{cases}$	—
`x`	Profile shift coefficient	$\in \mathbb{R}$	—
α_t	Transverse pressure angle	$\in (0, \pi]$	rad
α_{n0}	Normal pressure angle at reference circle	$\in (0, \pi]$	rad
β_b	Helix angle at base circle	$\in [0, \pi/2)$	rad
η_b	Base space width half angle	$\in [0, 2\pi)$	rad
φ_b	Position of involute at base circle at $z = 0$	$\in [0, 2\pi)$	rad

1. Introduction

The second part of this work addresses the mathematical description of involute gear flank and pitch deviations. The main idea is to use a new involute coordinate system introduced in part I of this article series [1]. This holistic 3D approach allows a convenient, easy and reliable evaluation of profile, helix and pitch deviations using the characteristic properties of the involute helicoid. 3D evaluations are required since measurement points are taken by 3D gear measurement instruments, which can be generally referred to as 3D coordinate measuring machines (CMMs) with tactile probing systems, optical probe heads or computed tomography devices. However, due to the generative principle between mating gears, the deviations are evaluated in the transverse plane, which is perpendicular to the gear axis. For helical gears, this is different to evaluations taken on other regular geometries such as planes, cylinders, cones or spheres, where the deviations are described perpendicular to the object's surface.

Another essential argument for the use of involute coordinates is that they provide for a nuanced examination of the generative motion between mating gears according to Euler's description [2]. The formulas used allow a function-orientated evaluation to be made that takes all effects of the gear kinematics into account, including those deviations which have until recently not been given full consideration. One prominent example is the correlation between pitch and profile deviations and the associated radial shift of evaluation ranges.

The basic geometry and fundamental rules for the evaluation of cylindrical involute gear deviations are described in numerous standards and guidelines [3–7]. But because these documents are lacking in computational details, manufacturers of CMMs and software developers make use of their own models and algorithms. Some of these have been in part described in [8–10] and they quite obviously rely on different approaches. This is why a software test service based on agreed and independent reference algorithms is strongly urged [11, 12].

This software test for cylindrical involute gear evaluations uses reference pairs consisting of synthetic measurement data and reference results. An independent evaluation software developed at the Physikalisch-Technische Bundesanstalt (PTB) is used to compute the reference results from the test data sets containing 3D stylus sphere center coordinates. The basic concepts and evaluation rules used in that software are explained in this paper. The procedures are in line with the definitions from the above mentioned international standards and guidelines. However, the descriptions feature a higher level of detail. All categories of gear deviation are computed using the 3D model introduced in [1] that can also be used for holistic inspection of various helical machine elements based on areal measurement data [13]. This way, the equations in this paper are capable of bridging between classical line based gear metrology and holistic areal inspection which goes beyond state of the art in this field.

The structure of this paper is as follows. Nomenclature starts with a comprehensive list of the symbols used in this paper that also includes the range of possible values and the unit assigned to each quantity. Section 2 recalls some fundamental principles of gear kinematics that form the prerequisites for function-oriented involute gear evaluation. The computation of involute gear deviations for individual measurement points using the coordinate system introduced in [1] is the subject of section 3, whereas in section 4 the rules are provided to computationally derive a set of evaluation parameters as described in the standards and guidelines from individual point deviations. The broad variety of evaluation options as discussed, for instance, in [6] is not included in this article.

Section 5 examines the influence of pitch deviations on the evaluation of profile deviations. This interaction can only be compensated when both pitch and profile measurements are evaluated within the same coordinate system. Involute coordinates allow this to be done in a convenient manner.

As the vast majority of running gears feature micro geometry corrections, also referred to as flank modifications, to ensure proper operating performance under load, section 6 shows how the most common modifications like reliefs and crowning can be covered by the introduced model.

Finally, section 7 concludes this paper and includes an outlook on further research activities aimed at establishing an online software test service for industrial users to provide certification for gear evaluation software.

2. Nomencalture

Involute gear evaluation relies on the fundamental principles of mating gears. The central characteristics are expressed in the gearing law.

> **Gearing law**
> An involute gear driven at a constant angular velocity is error-free if it produces a constant angular velocity in the mating gear as well.

The generative principle describes the fundamental kinematic principle of mating gears.

> **Generative principle**
> The motion of mating gears combines a rotational with a translational movement. When the driving wheel rotates with constant velocity it causes a linear translation of the contact point along the line of action which also shows constant velocity.

Correct involute gear evaluation directly follows from the demands posed by the gearing law and the generative principle.

> **Involute profile evaluation criterion**
> According to the generative principle, the evaluation of involute profile deviations must reference equidistant points along the length of roll, which correspond exactly to equally spaced rolling angles.

The central aspects of mating involute gears and their evaluation principle are illustrated in figure 1.

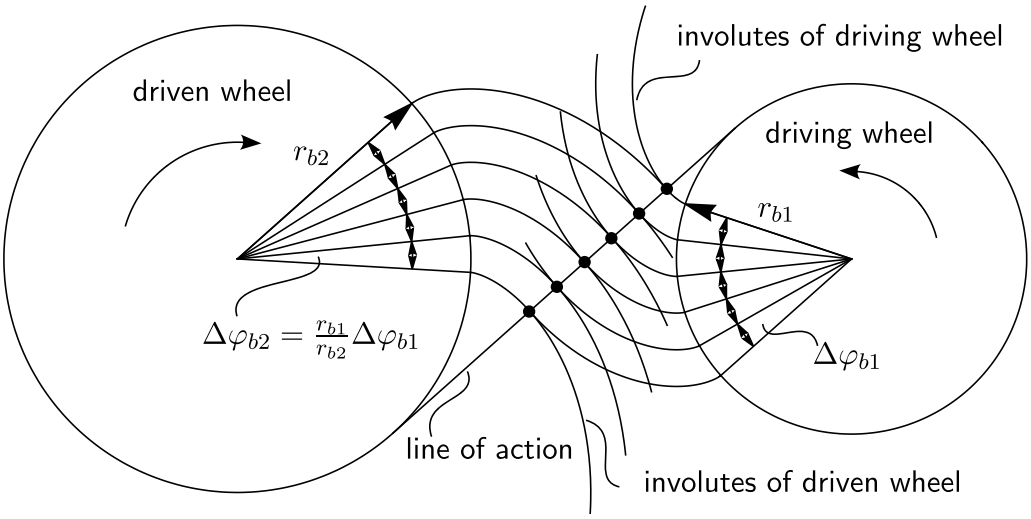

Figure 1. Mating gears. When the *driving wheel* with base radius r_{b1} rotates by $\Delta\varphi_{b1}$, it causes the *driven wheel* with base radius r_{b2} to rotate by $\Delta\varphi_{b2} = \frac{r_{b1}}{r_{b2}}\Delta\varphi_{b1}$. All contact points between the involutes of the driving and the driven wheels lie on the same straight line, the so-called *line of action*.

3. Involute gear deviations

Geometrical deviations of involute gear flanks are derived from the generative principle of mating gears. They are always described and evaluated in the gear's transverse plane. This is in contrast to other geometries, where deviations are expressed perpendicular to the object's surface.

Involute gear deviations are typically divided into profile, helix and pitch deviations (see figure 2). These three measurement tasks are sufficient to determine and to correct manufacturing errors for unmodified gears. Note that modern measurement techniques using optical or computed tomography systems allow the analysis of all measurement points taken on the gear flank. However, these measurement points have also to be handled using the classical evaluation cross sections.

In the discussion that follows, it is important to note that every individual measurement point is treated as an independent involute point as introduced in [1]. An involute point is expressed by five geometry parameters and three coordinates:

$$\texttt{InvPnt} = (\texttt{type}, \texttt{hand}, \texttt{flank}, r_b, c; \varphi_b, r, z). \qquad (1)$$

The constants `type`, `hand` and `flank` define the algebraic sign of the normal vector and hence the material side. r_b describes the size of the involute whereas $c = \tan(\beta_b)/r_b$ represents the radius-independent lead of the helix. The coordinates φ_b, r and z describe the 3D location of the individual point on an involute gear flank.

All deviations - whether of profile, helix or pitch - are calculated in involute coordinates, as these provide many advantages compared to Cartesian coordinates.

Measuring involute gears on CMMs presents us with two special challenges. The first relates to measurements taken on tactile CMMs and concerns the required stylus radius correction, i.e. translating stylus center point coordinates into corresponding surface points. The second issue involves the correction of the surface contact points, which are typically not perfectly located within the evaluation cross sections. These points have to be computationally shifted into the specified evaluation paths (see figure 2).

In the case of an involute curve, both challenges are quite easily overcome through the use of involute coordinates. As the involute curve is its own parallel curve, radius correction can be performed applying equation (22) from [1] as shown in figure 3.

One of the striking characteristics of the involute helical flank is that the z-component of the normal vector is constant on any location of the surface according to equation (17) in [1], namely

$$n_z = \texttt{type} \cdot \texttt{hand} \cdot \texttt{flank} \cdot \sin(\beta_b). \qquad (2)$$

Note that the actual normal vector on an involute profile with deviatons is in general not tangent to the base circle. However, the procedure described in [6] defines a reference involute to the nominal base radius that is best-fitted into the measurement points, i.e. the stylus sphere center points. The normal vector of each measurement point is then perpendicular to this reference involute and not to the actual profile with deviations. The effects resulting from this procedure are considered to be negligible.

After the necessary corrections of the measurement points have been performed, the individual point deviation $f_{y,i}$ can be calculated for each of the derived surface points.

Figure 4 illustrates the relation between the deviation $f_{y,i}$ of an individual measurement point p_i and its corresponding involute coordinate $\varphi_{b,i}$. Each measurement point

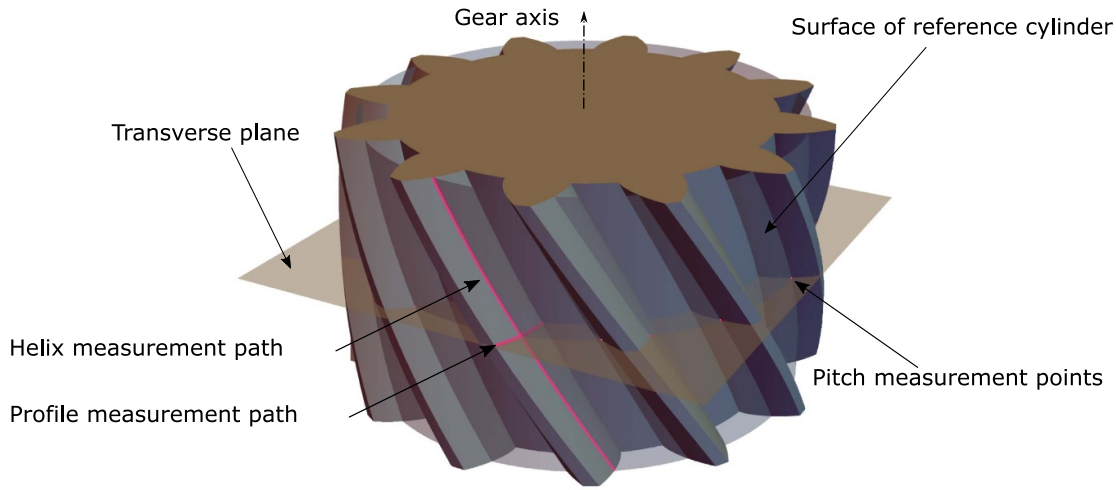

Figure 2. Cross sections and measurement tasks for the evaluation of cylindrical involute gears.

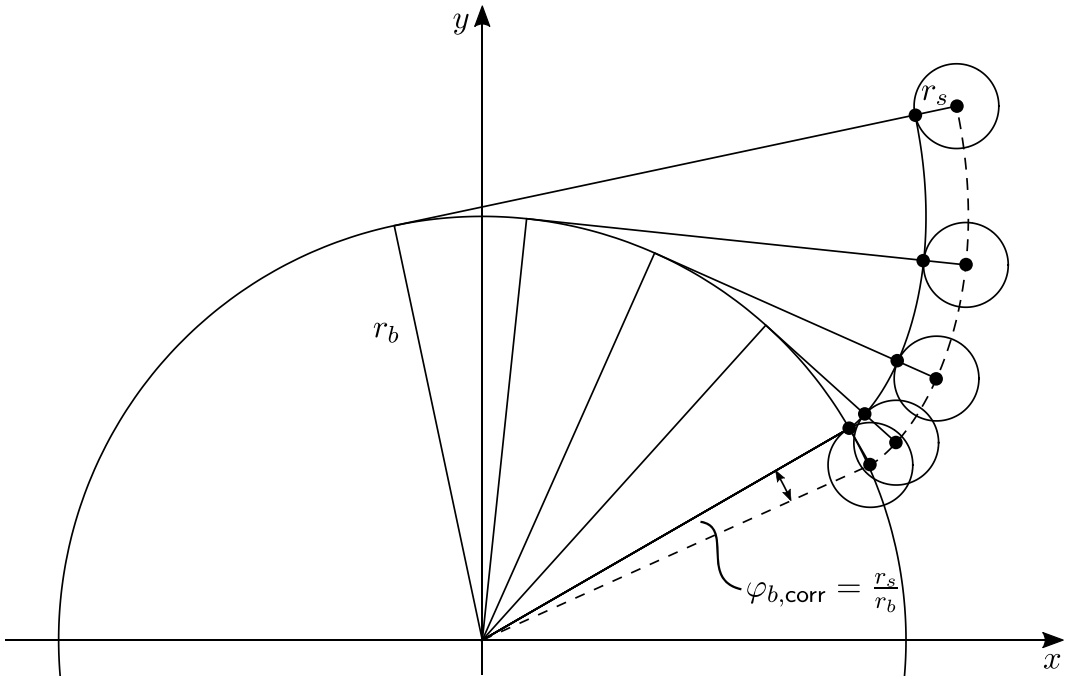

Figure 3. The offset curve of an involute is itself an involute with the same base radius. Its offset angle can easily be calculated as $\varphi_{b,\mathrm{corr}} = \frac{r_s}{r_b}$ with r_s denoting the stylus radius.

$$p_i = (\texttt{type}, \texttt{hand}, \texttt{flank}, r_b, c; \varphi_{b,i}, r_i, z_i) \tag{3}$$

is considered as belonging to a perfect involute with nominal base radius r_b whose angular position is rotated by $\Delta\varphi_{b,i}$. Considering only the constant `flank`, each deviation is easily calculated with the correct algebraic sign as follows:

$$f_{y,i} = \texttt{flank} \cdot r_b \cdot \Delta\varphi_{b,i} = \texttt{flank} \cdot r_b \cdot (\varphi_{b,\mathrm{ref}} - \varphi_{b,i}). \tag{4}$$

Following the traditional evaluation strategy, the reference angle $\varphi_{b,\mathrm{ref}}$ for each tooth should be chosen according to the approach described in [6]. For a holistic evaluation of involute gears, correlations between the profile and pitch deviations must be considered. The determination of the reference angles $\varphi_{b,\mathrm{ref}}$ and the evaluation of deviations is described in section 5.

In general, the algebraic sign of the deviation f_y does not correlate to plus or minus material. More precisely, for external gears a positive deviation $f_y > 0$ is understood as plus material and a negative deviation $f_y < 0$ as minus material. For internal gears the opposite is true, with $f_y > 0$ indicating minus material and $f_y < 0$ plus material (figure 4).

4. Derivation of standardized parameters from involute gear deviations

The preceding section described the calculation of deviations for individual points on the gear flank. This section deals with the determination of the most prominent evaluation parameters calculated from these pointwise deviations.

Given the great number of national and international standards and guidelines as well as the diversity of inspection rules applied by companies, this article can only concentrate on the fundamental evaluation methods. The enormous number of different evaluation ranges and options as well as their individual interpretation will not be covered here.

4.1. Profile evaluation

In this section the standardized profile evaluation [6] is presented independently of the effects resulting from a holistic 3D evaluation approach where correlations between pitch and profile are also considered. These correlations will be precisely described in section 5.

The deviations f_y are plotted against the nominal length of roll l_y, i.e. the length to the reference profile (dashed line in figure 4), in order to obtain the evaluation diagram for the calculation of all standardized parameters (slope, form, and total deviation, tip and root reliefs, crowning, etc).

For each measurement point $p_i = (\texttt{type}, \texttt{hand}, \texttt{flank}, r_b, c; \varphi_{b,i}, r_i, z_i)$ the corresponding length of roll $l_{y,i}$ is calculated by

$$l_{y,i} = \sqrt{r_i^2 - r_b^2} - f_{y,i}. \tag{5}$$

The example depicted in all the cases (a)–(d) in figure 4 yields the diagram shown in figure 5.

If the measurement points are not recorded following the involute profile evaluation criterion (see section 2), numerical correction has to be applied. This can take on particular importance when scanning mode is used on gear measuring devices or CMMs that do not follow the generative principle [14]. This is also strongly recommended in ISO 18653 [15].

The three most prominent evaluation parameters for profile deviations are

- Total profile deviation F_α,
- Profile slope deviation $f_{H\alpha}$,
- Profile form deviation $f_{f\alpha}$.

Different standards and guidelines may define different evaluation ranges for these quantities. However, the underlying computational rules described in this article are always the same.

In the case of a plain involute profile, the deviation within the specified evaluation range L_α is calculated by

$$F_\alpha = \max_i f_{y,i} - \min_i f_{y,i}. \tag{6}$$

Profile slope deviation $f_{H\alpha}$ is calculated by means of a linear least square fit considering the deviations inside the specified evaluation range L_α. Two points have to be remembered here:

- For historical reasons $f_{H\alpha}$ is defined as a length instead of an angle.
- In general, the evaluation range L_α used for computing the least squares line is different from the reference length L_{AE} in which $f_{H\alpha}$ is determined [6].

When m denotes the slope of the fitted least squares line, the profile slope deviation is

$$f_{H\alpha} = m \cdot L_{AE}. \tag{7}$$

According to [5, 6], profile slope deviation is deemed to be positive when the fitted least squares line (mean profile line) with slope m shows an increase in material toward the tooth tip, relative to the nominal involute. Otherwise it is negative (or zero). This applies to both external and internal gears.

Figure 5(a) shows the profile deviations of external gears. The diagram is plotted from root to tip in the direction of increasing length of roll. The material side is below the curve. Figure 5(b) shows the profile deviations of internal gears. Unlike the diagram for external gears, this diagram is plotted from tip to root, but also in the direction of increasing length of roll. The material side is above the curve.

The shape of an involute is defined solely by its base circle radius r_b. The relative base circle deviation $(r_{b,\mathrm{act}} - r_{b,\mathrm{nom}})/r_{b,\mathrm{nom}}$ is approximately proportional to the profile slope deviation (see figure 6) according to

$$\frac{f_{H\alpha}}{L_{AE,\mathrm{nom}}} \approx \frac{r_{b,\mathrm{act}} - r_{b,\mathrm{nom}}}{r_{b,\mathrm{nom}}}. \tag{8}$$

Note that equation (8) holds for external and internal gears as well as for left and right flanks. A larger base circle always results in a positive profile slope deviation according to the definition in [5, 6].

The profile form deviation $f_{f\alpha}$ is calculated from the extreme values of the residuals from the least squares line denoted by $f_{y,i}^{\mathrm{res}}$.

$$f_{f\alpha} = \max_i f_{y,i}^{\mathrm{res}} - \min_i f_{y,i}^{\mathrm{res}}. \tag{9}$$

4.2. Helix deviations

For each measurement point $p_i = (\texttt{type}, \texttt{hand}, \texttt{flank}, r_b, c; \varphi_{b,i}, r_i, z_i)$ the deviation $f_{y,i}$ from equation (4) is plotted against its z-coordinate z_i. In this diagram, all helix deviation parameters can be determined.

The three most prominent evaluation parameters for helix deviations are

- Total helix deviation F_β,
- Helix slope deviation $f_{H\beta}$,
- Helix form deviation $f_{f\beta}$.

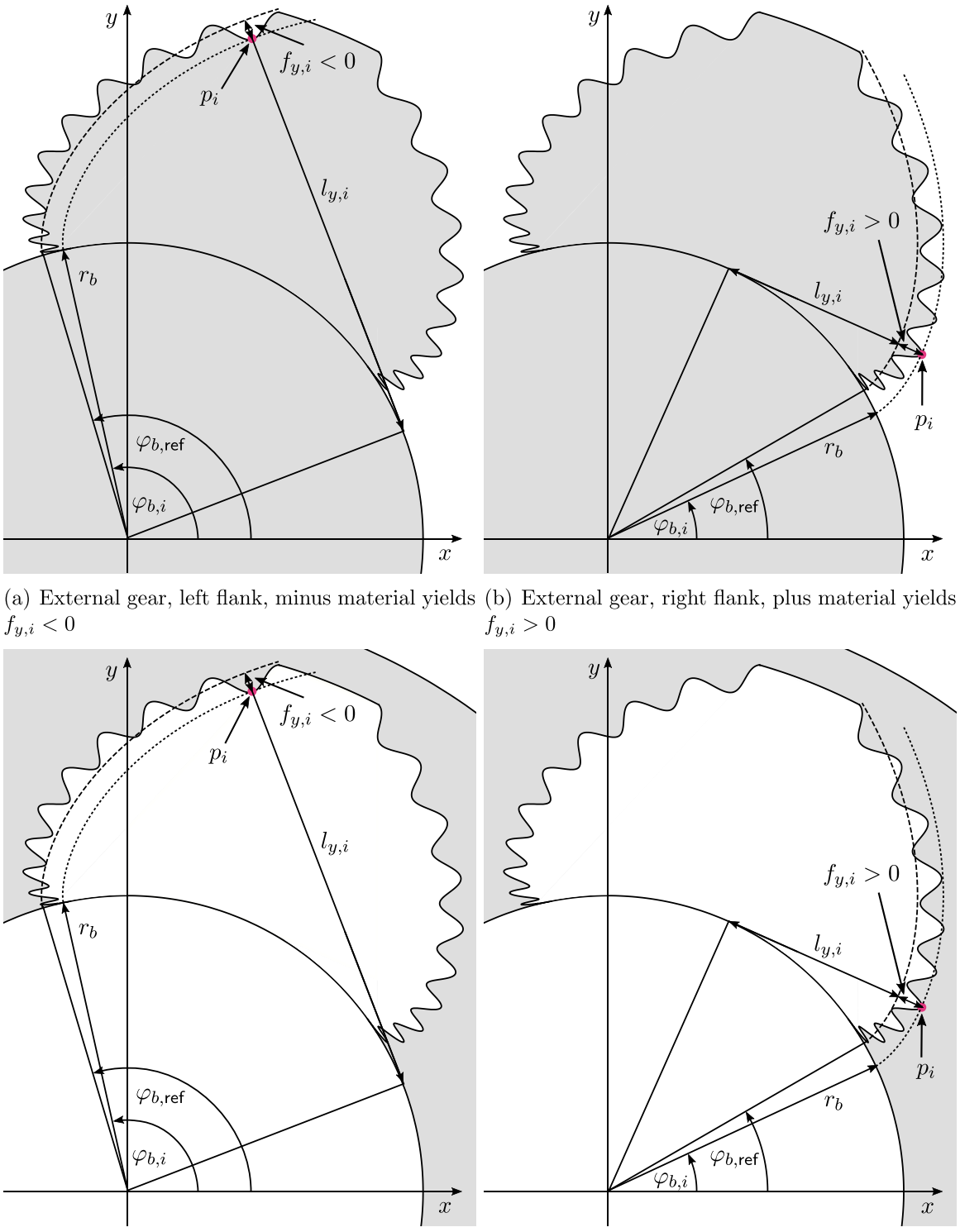

(a) External gear, left flank, minus material yields $f_{y,i} < 0$

(b) External gear, right flank, plus material yields $f_{y,i} > 0$

(c) Internal gear, left flank, plus material yields $f_{y,i} < 0$

(d) Internal gear, right flank, minus material yields $f_{y,i} > 0$

Figure 4. Algebraic sign of deviations for all gear `type` and `flank` cases.

Different standards and guidelines may define different evaluation ranges for these quantities. However, the underlying computational rules described in this article are always the same.

In the case of an unmodified helix, the deviation within the specified evaluation range L_β is calculated by

$$F_\beta = \max_i f_{y,i} - \min_i f_{y,i}. \tag{10}$$

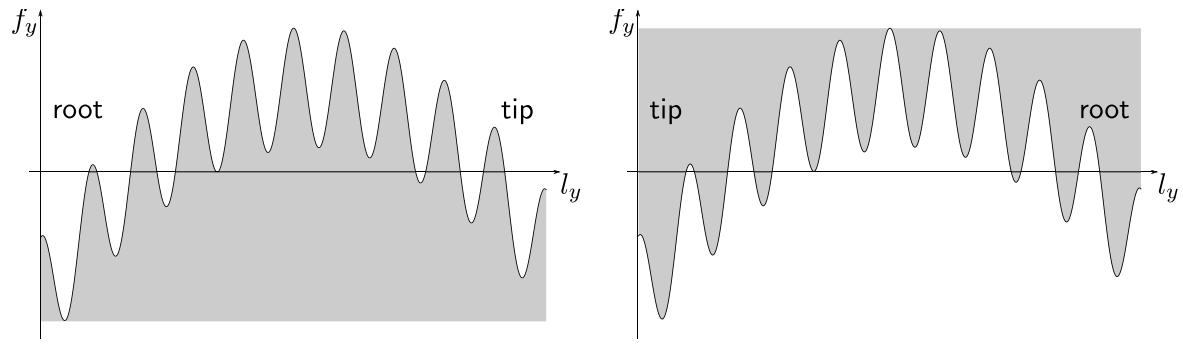

(a) External gear, material side is below the curve, root is left, tip is right

(b) Internal gear, material side is above the curve, root is right, tip is left

Figure 5. Profile deviation f_y against nominal length of roll l_y. When the gear type (external or internal) is changed, not only does the material side switch but the tip and root are also reversed.

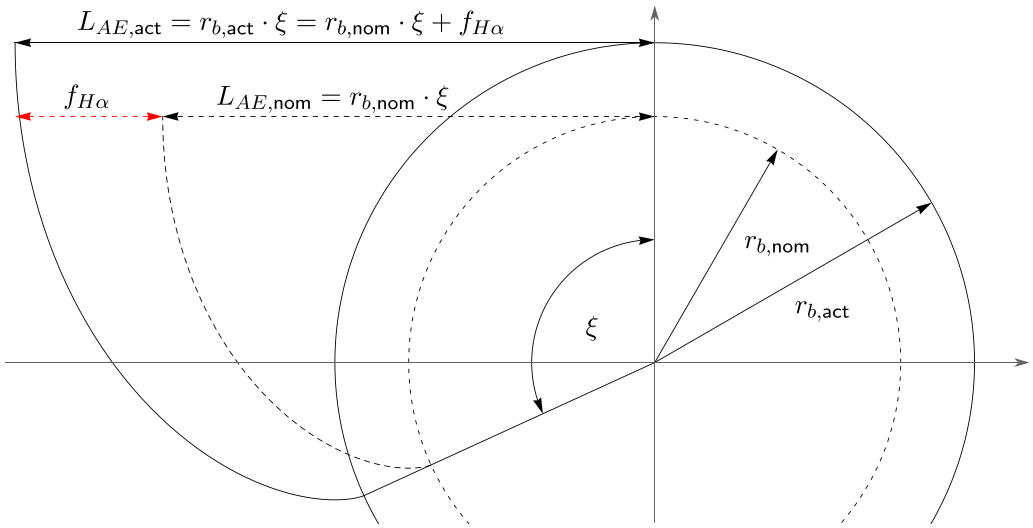

Figure 6. Every profile deviation may be interpreted as local base circle deviation. This leads to equation (8).

Helix slope deviation $f_{H\beta}$ is calculated by means of a linear least square fit considering the deviations inside the specified evaluation range L_β. Two points have to be remembered here:

- For historical reasons $f_{H\beta}$ is defined as a length instead of an angle.
- In general, the evaluation range L_β used for computing the least squares line is different from the reference length b in which $f_{H\beta}$ is determined.

When m denotes the slope of the fitted least squares line, the helix slope deviation is

$$f_{H\beta} = m \cdot b\,. \tag{11}$$

According to [5, 6], helix slope deviation is deemed to be positive when the actual helix angle is larger than the nominal helix angle. For spur gears helix slope deviation is positive when the actual helix is right-handed and negative if it is left-handed. This applies to both external and internal gears as well as to left and right flanks.

The relation of helix slope deviation and actual base helix angle is depicted in figure 7 and explicitly given by equation (12).

$$f_{H\beta} = b \cdot (\tan\beta_{b,\mathrm{act}} - \tan\beta_{b,\mathrm{nom}}). \tag{12}$$

The helix form deviation $f_{f\beta}$ is calculated from the extreme values of the residuals $f_{y,i}^{\mathrm{res}}$ from the least squares line.

$$f_{f\beta} = \max_i f_{y,i}^{\mathrm{res}} - \min_i f_{y,i}^{\mathrm{res}}. \tag{13}$$

4.3. Pitch deviations

In this section, the evaluation of transverse pitch deviations is described. The transverse pitch is defined to be the arc length between two successive tooth flanks of equal direction on the reference radius r_0 (see figure 8). The first pitch is defined between the last and the first tooth.

The individual cumulative pitch deviation $F_{p,i}$ at the left or right flank of tooth number i is referenced to the actual position

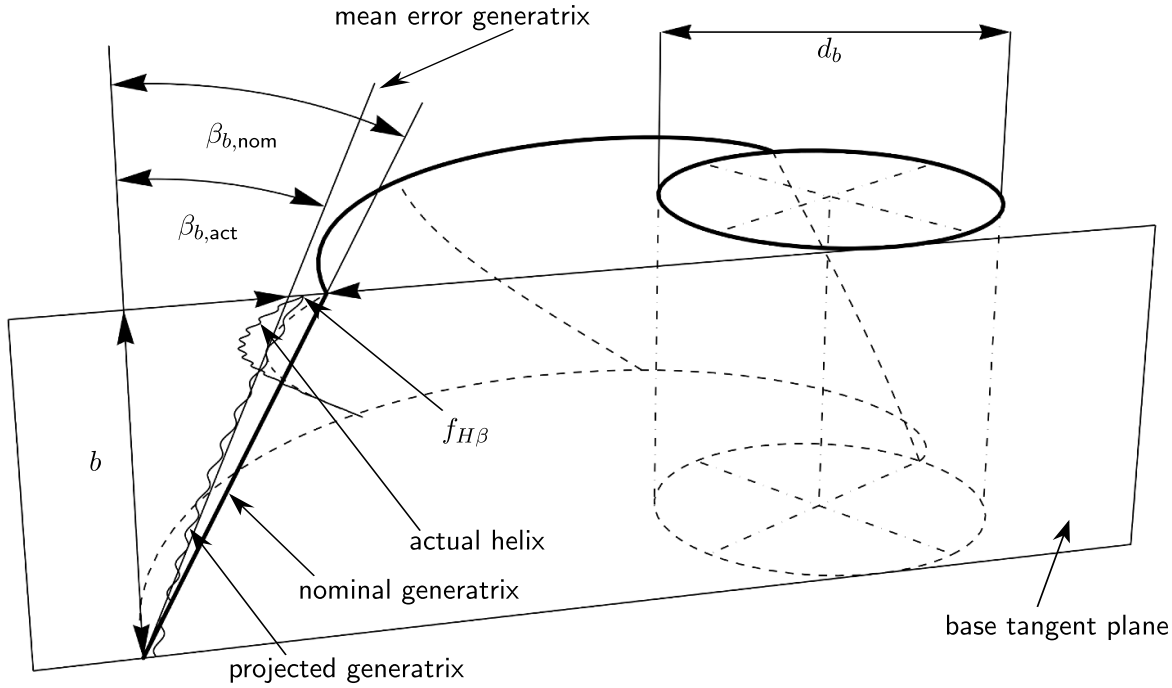

Figure 7. Base cylinder with involute helicoid. For each measurement point, the helix deviation is evaluated in a direction tangent to the base circle according to equation (4). If all the deviations are rotated into a common base tangent plane, the resulting curve can be considered as a projected generatrix and the relation in equation (12) becomes obvious.

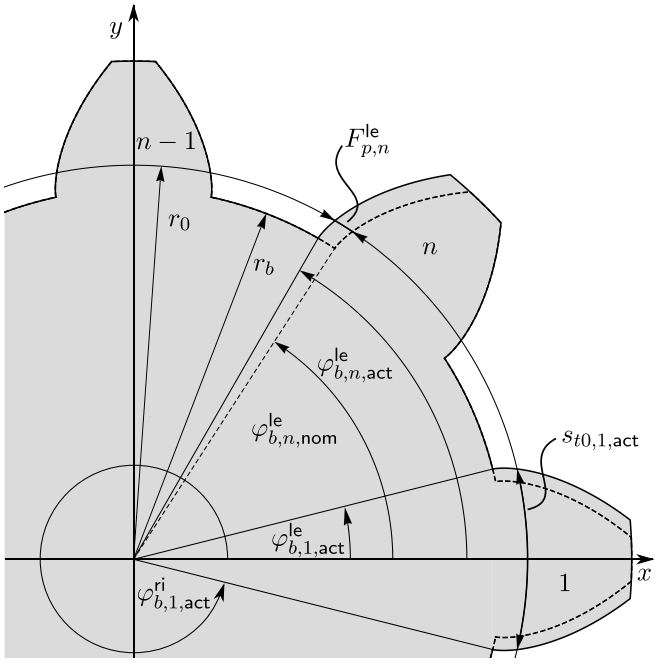

Figure 8. Definitions of cumulative pitch deviations and tooth thickness.

of the first tooth $\varphi_{b,1,\mathrm{act}}$, which defines the nominal positions of all teeth $\varphi_{b,i,\mathrm{nom}}$ (see section 4.3 in [1]). This also allows profile shift or any other tooth thickness modification to be taken into account. $F_{p,i}$ is calculated by

$$F_{p,i} = r_0(\varphi_{b,i,\mathrm{nom}} - \varphi_{b,i,\mathrm{act}}), \tag{14}$$

where[1]

$$\varphi_{b,i,\mathrm{nom}} = \varphi_{b,1} - (i-1)\frac{2\pi}{n} \bmod 2\pi. \tag{15}$$

Figure 9 illustrates that in general there is no correlation between the algebraic sign of $F_{p,i}$ and plus or minus material on the flank.

The individual single pitch deviation $f_{p,i}$ is derived as follows:

$$f_{p,1} = F_{p,1} - F_{p,n} = -F_{p,n} \tag{16}$$

$$f_{p,i} = F_{p,i} - F_{p,i-1} \quad (2 \leqslant i \leqslant n). \tag{17}$$

In order to avoid cumulative errors, it is recommended to calculate the individual single pitch deviations $f_{p,i}$ from the individual cumulative pitch deviations $F_{p,i}$.

If the pitch deviations are to be evaluated on a circle with a radius r_v that differs from the reference circle radius, the individual cumulative pitch deviations can easily be calculated by

$$F^v_{p,i} = r_v(\varphi_{b,i,\mathrm{nom}} - \varphi_{b,i,\mathrm{act}}). \tag{18}$$

The cumulative pitch deviation F_p is defined as

$$F_p = \max_i F_{p,i} - \min_i F_{p,i}. \tag{19}$$

[1] The *modulo* operator mod 2π calculates the remainder of the division of any real number by 2π. This remainder always lies in the interval $[0, 2\pi)$.

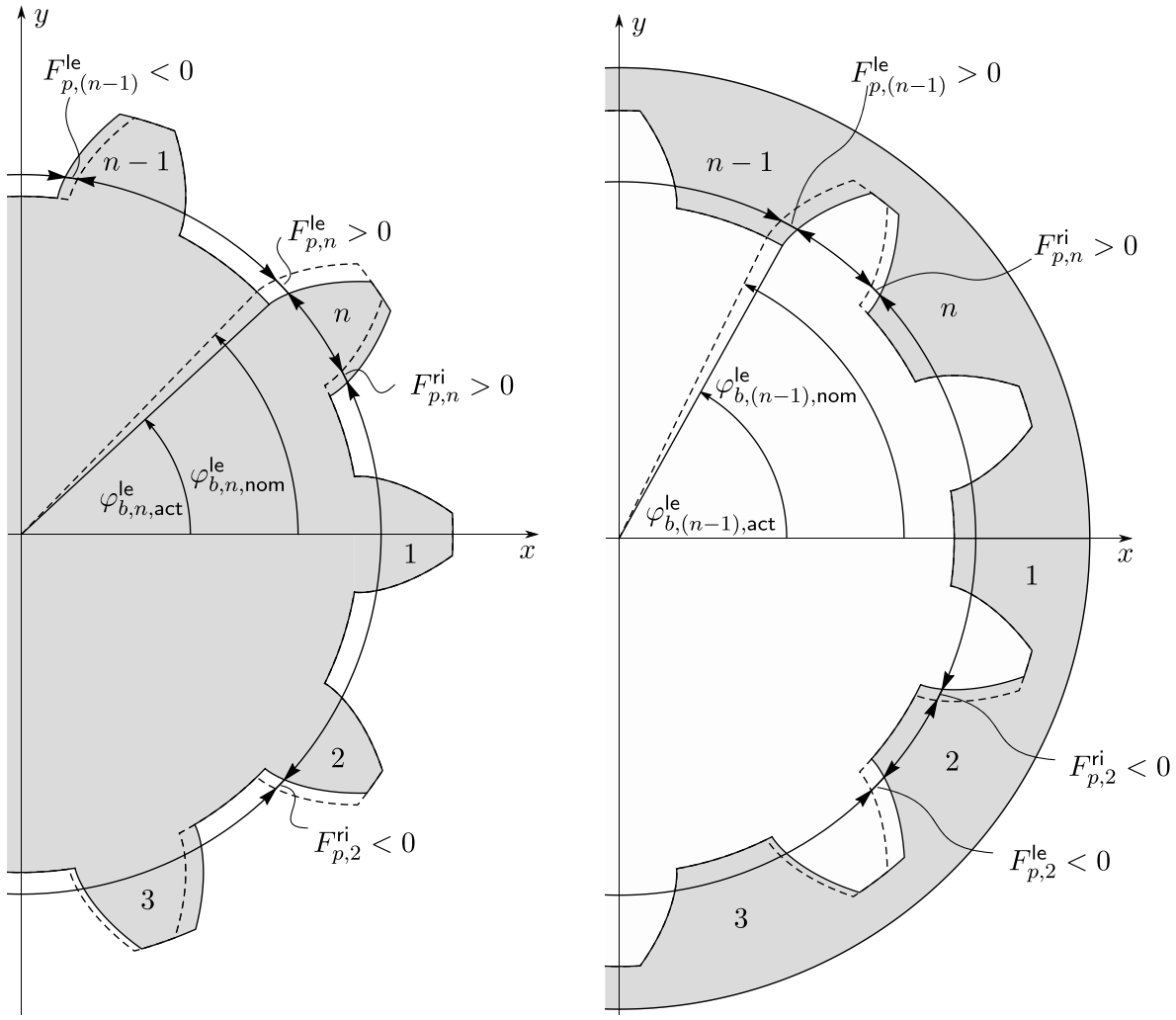

(a) External gear (b) Internal gear

Figure 9. Individual cumulative pitch deviations $F_{p,i}$. The algebraic sign according to equation (14) depends on the absolute position of the flank related to its nominal position and does not necessarily correspond to plus or minus material.

The single pitch deviation f_p is

$$f_p = \max |f_{p,i}|. \tag{20}$$

In contrast to the calculations, values in diagrams can be shifted by an absolute value based on individual conventions. The most common representation follows DIN 3960 [4] (withdrawn since 2012) and defines $F_{p,n} = 0$. Note that this does not affect the values of F_p and f_p.

4.4. Tooth thickness

The actual transverse tooth thickness $s_{t0,i}$ on tooth number i is an absolute measure. It is defined to be the arc length between the left and right flanks of tooth number i on the reference radius r_0 (see figure 10) and is evaluated according to

$$s_{t0,i} = r_0 \left(\Delta\varphi_{b,i} - 2 \cdot \mathtt{type} \cdot \mathrm{inv}\alpha_t(r_0)\right), \tag{21}$$

where

$$\Delta\varphi_{b,i} = \mathtt{type}\left(\varphi^{le}_{b,i,act} - \varphi^{ri}_{b,i,act}\right) \bmod 2\pi. \tag{22}$$

4.5. Calculation of a stylus sphere radius for double-flank contact

Some important gear measurands are defined to be measured with a stylus sphere simultaneously touching both flanks of a tooth space on a given diameter of the gear. Such measurements are, for example, used to evaluate the gear's runout deviations as well as the dimension over and between balls which allows to draw conclusions on the tooth thickness. This requires the calculation of a theoretical stylus sphere radius.

Let the contact radius r on the gear flanks be given and let

$$\alpha_t(r) = \arccos\left(\frac{r_b}{r}\right) \tag{23}$$

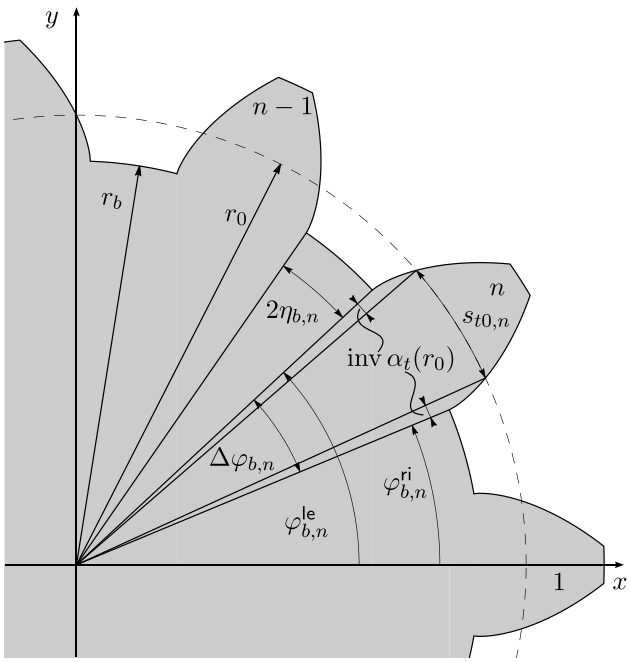

Figure 10. Definitions of angles involved in tooth thickness calculations.

be the pressure angle at this radius r. When

$$\eta_b = \frac{\pi - \mathtt{type}\cdot 4\cdot \mathtt{x}\cdot \tan\alpha_{n0}}{2n} - \mathtt{type}\cdot \mathrm{inv}\alpha_t(r_0) \qquad (24)$$

denotes the base space width half angle of the gear, the radius r_s of the stylus sphere touching both flanks simultaneously on a cylinder with radius r is calculated by solving

$$r_s = \frac{r_b}{\cos\beta_b}\left(\tan(\eta_b - cr_s\sin\beta_b + \mathtt{type}\cdot\tan\alpha_t(r)) - \mathtt{type}\cdot\tan\alpha_t(r)\right). \qquad (25)$$

Note that equation (25) is implicit and transcendental with respect to r_s and must be solved by a numerical approximation method such as described in [16]. However, in the case of a spur gear ($\beta_b = 0$), a direct solution is given by

$$r_s = r_b\left(\tan(\eta_b + \mathtt{type}\cdot\tan\alpha_t(r)) - \mathtt{type}\cdot\tan\alpha_t(r)\right). \qquad (26)$$

The theoretical derivation of equation (25) can be found in [17].

4.6. Runout

Runout can be determined following two different approaches. One uses direct measurements in double-flank contact, the other is based on calculations from pitch deviations.

The direct approach yields a set of n sphere center coordinates (x_i, y_i, z_i) from measurements in double-flank contact located in one transverse plane $z_i = z_j$ for $i,j = 1,\ldots,n$. The radial distances to these stylus sphere center coordinates then lead to the individual values $F_{r,i}$ with

$$F_{r,i} = \sqrt{x_i^2 + y_i^2} \qquad \text{for} \quad i = 1,\ldots,n. \qquad (27)$$

The indirect approach is based on the set of $2n$ angles $\varphi^{\mathrm{le}}_{b,i}$ and $\varphi^{\mathrm{ri}}_{b,i}$ of the left and right flanks as derived from pitch deviations. Following the definition of tooth space numbers (see figure 2 in [1]), for external gears the actual value of the ith space width half angle $\eta_{b,i}$ is calculated with

$$\eta_{b,1} = \frac{\varphi^{\mathrm{ri}}_{b,n} - \varphi^{\mathrm{le}}_{b,1}}{2} \bmod 2\pi \qquad (28)$$

and

$$\eta_{b,i} = \frac{\varphi^{\mathrm{ri}}_{b,i-1} - \varphi^{\mathrm{le}}_{b,i}}{2} \bmod 2\pi \qquad \text{for} \quad i = 2,\ldots,n. \qquad (29)$$

Accordingly, for internal gears $\eta_{b,i}$ is calculated by

$$\eta_{b,1} = \frac{\varphi^{\mathrm{le}}_{b,n} - \varphi^{\mathrm{ri}}_{b,1}}{2} \bmod 2\pi \qquad (30)$$

and

$$\eta_{b,i} = \frac{\varphi^{\mathrm{le}}_{b,i-1} - \varphi^{\mathrm{ri}}_{b,i}}{2} \bmod 2\pi \qquad \text{for} \quad i = 2,\ldots,n. \qquad (31)$$

Based on each actual angle $\eta_{b,i}$, the corresponding contact radius r_i for double-flank contact in the ith tooth space may now be derived by numerically solving equation (25) with a theoretical stylus sphere radius r_s. This theoretical value of r_s may either be given by technical specifications for the measurement task or can be calculated based on the nominal gear geometry as described in section 4.5. Once the contact radius r_i is determined for each tooth space, the corresponding radial distance to the stylus sphere center $F_{r,i}$ is obtained by

$$F_{r,i} = \sqrt{r_b^2 + (r_b\tan\alpha_t(r_i) + \mathtt{type}\cdot r_s\cos(\beta_b))^2} \quad \text{for} \quad i = 1,\ldots,n. \qquad (32)$$

For reference, see [17, figures 6, 7 and equation (46)].

The runout deviation F_r is defined as

$$F_r = \max F_{r,i} - \min F_{r,i}. \qquad (33)$$

Note that the results of both methods are only comparable if the same stylus sphere radius r_s is used for both the measurement in the direct approach and the calculation in the indirect approach. In practice, both methods may still lead to different outcomes as the contact points for the underlying measurements are located on different radii, which will lead to different form deviation effects.

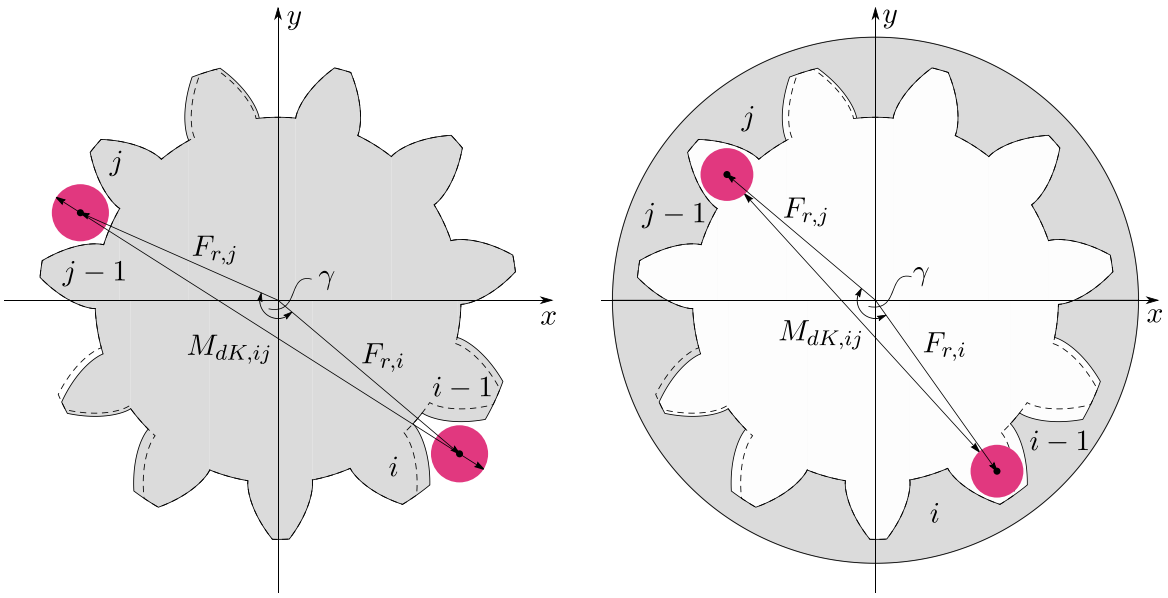

(a) External gear (b) Internal gear

Figure 11. The dimension over (or between) balls $M_{dK,ij}$ depends on the actual pitch of the gear represented by the angle γ.

4.7. Dimension over and between balls

Taking the results from section 4.6, the radial single-ball dimension $M_{rK,i}$ for the tooth space number i is computed with

$$M_{rK,i} = F_{r,i} + \texttt{type} \cdot r_s. \tag{34}$$

However, the calculation of the dimension over (or between) balls $M_{dK,ij}$ must take into account the actual pitch of the gear expressed in terms of $\varphi^{\text{le}}_{b,i}$ and $\varphi^{\text{ri}}_{b,i-1}$ as well as $\varphi^{\text{le}}_{b,j}$ and $\varphi^{\text{ri}}_{b,j-1}$ with j denoting the tooth space opposite to the ith tooth space. More precisely, we choose

$$j = \begin{cases} i + \dfrac{n}{2} & \text{for even } n, \\ i + \dfrac{n-1}{2} & \text{for odd } n. \end{cases} \tag{35}$$

For the triangle shown in figure 11, we have

$$\gamma = \frac{\varphi^{\text{le}}_{b,i} + \varphi^{\text{ri}}_{b,i-1}}{2} - \frac{\varphi^{\text{le}}_{b,j} + \varphi^{\text{ri}}_{b,j-1}}{2}, \tag{36}$$

where both terms should be reduced mod 2π if necessary, and derive from the law of cosines that

$$M_{dK,ij} = \sqrt{F^2_{r,i} + F^2_{r,j} - 2F_{r,i}F_{r,j}\cos(\gamma)} + \texttt{type} \cdot 2r_s. \tag{37}$$

5. Correlation between profile and pitch deviation

Pitch deviations can falsify the profile evaluation if not properly separated from one another. For the sake of simplicity this is explained on an ideal involute shifted by a pitch deviation.

In figure 12 the actual profile deviates from the nominal profile only by a pitch error $r_0 \cdot \Delta\varphi_b$. The profile error is evaluated in terms of length of roll along the line of action. Each measurement point of the profile measurement is evaluated against the nominal profile. The effect is that the actual point and the corresponding nominal point of the profile are located on different circles with radii r_{act} and r_{nom} leading to a shift of the complete profile measurement by the amount of the pitch error. This means that the profile will be evaluated in a different evaluation range than the one specified, with this range shifted in terms of length of roll by

$$l_{y,\text{act}} = l_{y,\text{nom}} + r_b \cdot \Delta\varphi_b \tag{38}$$

and in the radial direction by

$$r_{\text{act}} = r_b\sqrt{1 + (\tan(\alpha_t(r_{\text{nom}})) + \Delta\varphi_b)^2}. \tag{39}$$

The active profile corresponding to the evaluation ranges on the nominal and actual profiles are depicted in red in figure 12.

A suitable method for correcting this influence on the profile evaluation based on individual reference profiles for each tooth is explained in VDI 2612 Part 1 [6].

6. Flank modifications

Micro geometry corrections (also referred to as flank modifications) are used to compensate for the elastic deformation of running gears under load. The most prominent modifications are crowning and slope modification as well as reliefs in both the profile and helix directions. This leads to intended deviations from the ideal involute helicoid that must be considered for a proper failure analysis.

VDI 2612 Part I provides a broad variety of evaluation rules for the inspection of modified profiles and helices on involute gears [6]. These rules build upon the standard procedure based on equations (4) and (5) from sections 3 and 4 in this

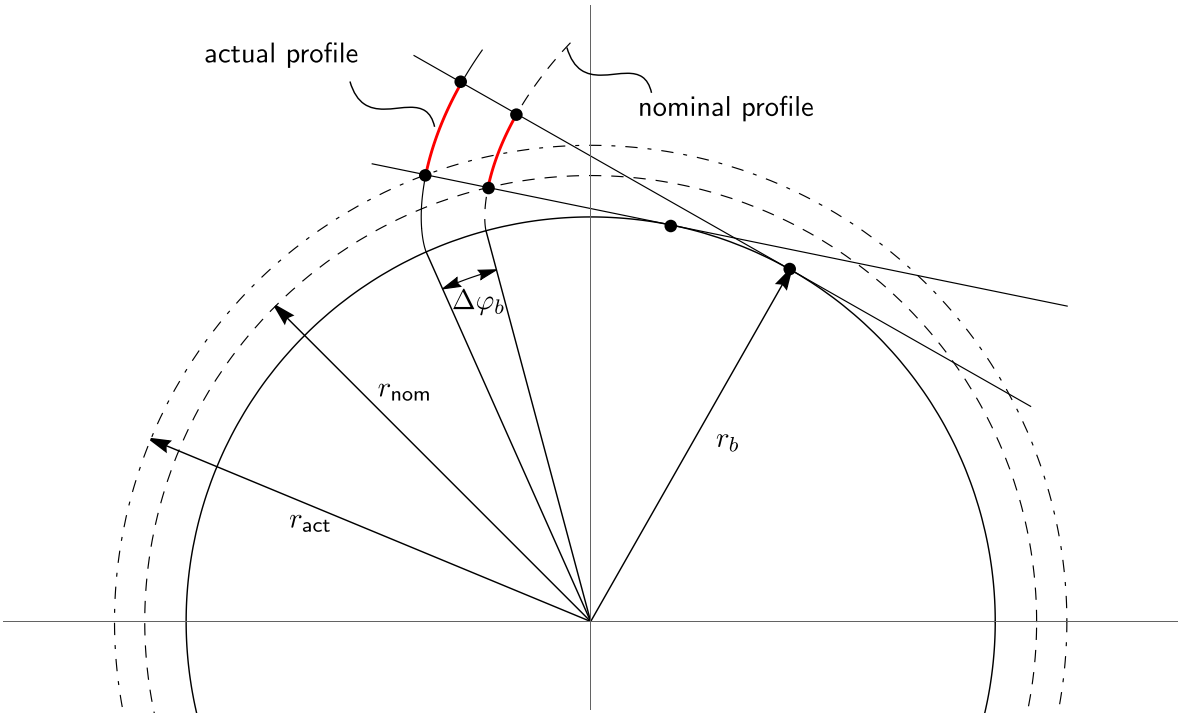

Figure 12. Correlation between profile and pitch deviation.

work. The characteristics of modifications are then treated by evaluating the derived deviations in separated ranges and with varied regression elements (e.g. parabolas instead of straight lines).

Special attention is to be paid when several flank modifications are combined. Although this is very common in gear production, standards and guidelines still lack precise evaluation rules.

7. Conclusion and outlook

The geometrical and computational basics for the evaluation of cylindrical involute gear measurements on CMMs have been described. The models and formulas are based on the fundamental gear kinematics and a 3D description using an involute gear coordinate system introduced in [1].

The presented equations form the basis of PTB's software test service to be implemented in its online validation system, TraCIM [18], as part of an ongoing research project (https://tracim.ptb.de). This service will provide independent test data sets for profile, helix and pitch deviations on involute gears. The data sets can be evaluated by manufacturers of CMMs and software developers to test their own evaluation algorithms against PTB's reference results. This will enable gear metrology service providers to certify their software for the first time and to reliably quantify the accuracy of their algorithms.

The software test service will also cover the evaluation of involute gears featuring all possible combinations of flank modifications as only briefly described in section 6. Details on evaluating deviations of modified gears will be the subject of future publications.

Data availability statement

No new data were created or analysed in this study.

ORCID iD

Martin Stein https://orcid.org/0000-0001-8729-8310

References

[1] Härtig F and Stein M 2019 3D involute gear evaluation—part I: workpiece coordinates *Measurement* **134** 569–73
[2] Euler L 1758 De constructione aptissima molarum alatarum *Novi Comment. Acad. Sci. Petropol.* **4** 41–108
[3] ISO 21771:2007-09 2007 *Gears—Cylindrical Involute Gears and Gear Pairs—Concepts and Geometry* (International Organisation for Standardization)
[4] DIN 3960:1987-03 *Definitions, Parameters and Equations for Involute Cylindrical Gears and Gear Pairs (Withdrawn)*
[5] ISO 1328-1:2013-09 2013 *Cylindrical Gears—ISO System of Flank Tolerance Classification—Part 1: Definitions and Allowable Values of Deviations Relevant to Flanks of Gear Teeth* (International Organisation for Standardization)
[6] VDI/VDE 2612 *Part 1:2018-11 Measurement and Testing of Gears—Evaluation of Profile and Helix Measurements on Cylindrical Gears with Involute Profile*
[7] VDI/VDE 2613:2003-12 *Pitch and Runout Testing on Gearings—Cylindrical Gears, Whormwheels (SIC!), Bevel Gears*
[8] Lotze W 2005 *Zahnradmessung mit Koordinatenmessgeräten* (Dresden: Eigenverlag)
[9] Goch G, Ni K, Peng Y and Guenther A 2017 Future gear metrology based on areal measurements and improved holistic evaluations *CIRP Ann.-Manuf. Technol.* **66** 469–74

[10] Zelený V, Linkeová I, Sýkora J and Skalník P 2019 Mathematical approach to evaluate involute gear profile and helix deviations without using special gear software *Mech. Mach. Theory* **135** 150–64
[11] Härtig F 2006 Certificate for involute gear evaluation software *Fall Technical Meeting* (American Gear Manufacturers Association)
[12] Lübke K and Stein M 2019 Gear metrology according to ISO 1328-1: variety of evaluation strategies for cylindrical involute gears and verification of corresponding algorithms *7th GETPRO Int. Conf. on Gearbox Production (Würzburg, Germany)*
[13] Stein M, Keller F and Przyklenk A 2021 A unified theory for 3D gear and thread metrology *Appl. Sci.* **11** 7611
[14] Härtig F 2005 Typische Fehler beim Messen von Zylinderrädern *VDI-Ber.* **1880** 91–98
[15] ISO 18653:2003-12 2003 *Gears—Evaluation of Instruments for the Measurement of Individual Gears* (International Organisation for Standardization)
[16] Press W H, Teukolsky S A, Vetterling W T and Flannery B P 2007 *Numerical Recipes 3rd edn: The Art of Scientific Computing* (Cambridge: Cambridge University Press)
[17] Stein M and Härtig F 2021 3D involute gear evaluation—supplement: measurements in double-flank contact *Measurement* **176** 109079
[18] Wendt K, Franke M and Härtig F 2015 *Validation of CMM Evaluation Software Using Tracim (Series on Advances in Mathematics for Applied Sciences* vol 86*)* (Singapore: World Scientific Publishing) pp 392–9